A catalytic approach to synthesis of PLP analogs and other environmental protocols in a single handed CaO/TiO$_2$ green nanoparticle

Sk Jahir Abbas[a], P.V.R.K. Ramacharyulu[a], Hsin-Hsi Lo[a], Sk Imran Ali[b], Shyue-Chu Ke[a],*

[a] Department of Physics, National Dong Hwa University, Hualien, 97401, Taiwan
[b] Department of Materials and Environmental Chemistry, Stockholm University, SE-106 91 Stockholm, Sweden

A B S T R A C T

As our precursory stage we have focus straight forward on clean catalytic approach for the production of C3 substituted pyridoxal-5′-phosphate analogues of vitamin B$_6$, and other environmental protocols like photocatalytic activity, green fossil fuels and c–c coupling using efficient biocompatible eggshell related unrivalled materials which show versatility of the catalytic effect on different inorganic support. The eggshell immobilized nanoparticles have encouraging relevance in creation of new molecules and can advantageously be studied by various spectroscopic, thermal and elemental analyses like powder X-ray diffraction (XRD), Raman spectroscopy, UV–vis, Scanning electron microscopy (SEM), Energy dispersive X-ray analysis (EDX), X-ray photoelectron spectroscopy (XPS) and Brunauer-Emmett-Teller (BET) surface area analysis. The elucidate nature of nanoparticles offer: more active site acts as lewis acid, vacancies on the catalyst surface and good to better yield of C3 substituted deoxy and 2-nor deoxy coenzyme pyridoxine (PN), coupling products propargylamines (PA), photo degrading enhancement of MB and nucleophilic substituted fatty acid (BD). This enzyme cofactor explore molecular synthons to synthetic equivalent: 3-deoxy and 2-nor-3-deoxy pyridoxal (PL), pyridoxal oxime (PO), pyridoxamine (PM) and mono phosphate derivative of 3-deoxyPM, 3-deoxyPL respectively and chemistry of selective oxidation and schiff base mechanism was studied and complemented through combined experimental and theoretical molecular orbital calculation consequently. The heterogeneous catalyst has strong selective ability towards selective reducing pyridine diester, bioactive intermediates substances and holds vast potential towards separation for the photogenerated electron-hole pairs and renewable, nontoxic, biodegradable green fossil fuels. The catalyst including environmental concern is reapplicable and strong impressive that can unfold the space of worthy metal component widely and facilitate the scope to take a vital role in different fileds like catalysis, biochemistry, nanoscience, energy and materials science.

© 2017 Elsevier B.V. All rights reserved.

1. Introduction

A wind of breathlessness is surrounded by every inch of land due to ascending cosmic heat and descending energy. The scientific communities become tempted to flourish abundant green materials from the natural and artificial resources which would be in grip of people, and prompt to apply [1,2]. A sharp research on these green raw materials is going on restlessly in order to provide a trauma free respiration as well as to conserve at least a single bit of energy for today's children and broad aspect for our future generation [3,4]. We are wonder enough with this noble thought of

scientists group, as consequence the mass of current century is impacted profusely [5–7].

Being capable of surprising physical properties and activities in biological system the chemistry of pyridoxal, pyridoxine and pyridoxamine analogues and phosphate forms i.e. pyridoxal-5′-phosphate (PLP), pyridoxine-5′-phosphate (PNP) and pyridoxamine-5′-phosphate (PMP), the very components of vitamin B6 have drawn vast impression to the field of enzymology and biochemical research for last few eras [8–10]. Numerous studies confirmed that the functional property of functionalized vitamers has supported many biochemical challenges, enzymatic activities and intermediate radicals which has been kept its distinction [8] see Fig. 1 (1–4). C3 substituted vitamers is much more consideration to the pharmaceutical chemists community for the studies enzymatic chemistry and then into the exploration of novel activities [11]. The

* Corresponding author.
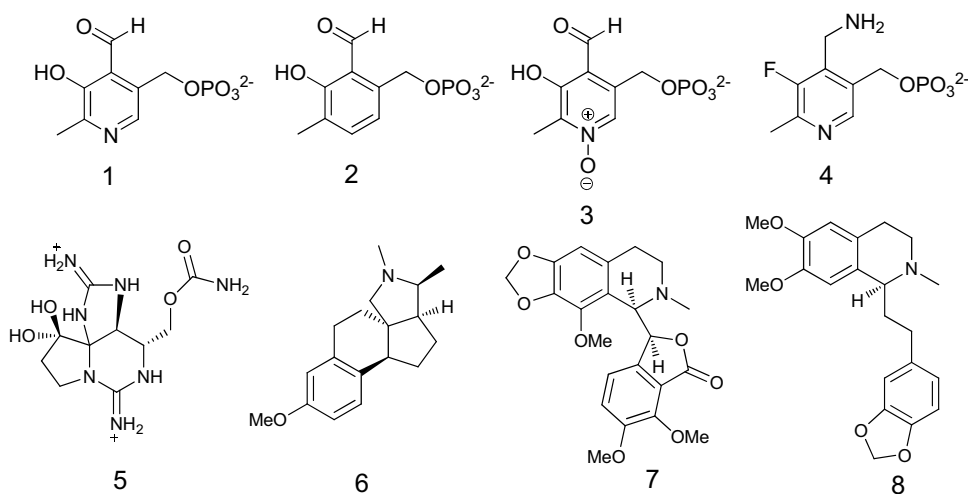 *E-mail address:* ke@mail.ndhu.edu.tw (S.-C. Ke).

Fig. 1. Structural presentation of representative coenzyme, natural and bioactive analogues.

reported methods on C3 modification backbones of coenzyme are limited till date and approaches are confined in various cases [12].

Since several years by observing the relentless utilization of dyes and pigments in dyeing industries the World Bank reported that plentiful oozing of these dyes effluents causes abundant aquatic pollution [13,14]. Lack of smooth formation, high thermal and photo stability of synthetic dyes, it is quite uneasy to make lower rank of the toxicity and carcinogenesis of dyes. Consequently, pollution control is in great demand [15,16]. Since the dawn of the expressive procedure of the advanced oxidation processes and heterogeneous photocatalysis came in existence, the utilization of metallic and nonmetallic doping elements are considered among effective and promising degrading organic pollutants [17,18].

In another way virgin nature becomes poisonous with men's aware deed. So the concept of discovering any available possibilities of nontoxic diesel in place of conventional fuel is a new edition in scientist's ever thinking. Excellent outcome is biodiesel along with its production and development for having renewability, potential of deducing greenhouse gas and inhibition soot formation causing less air pollution [19,20]. Biodiesel comprises of waste oil is apt in its any form. Therefore extensive investigation is required for producing better qualified and more quantities biodiesel by using extraordinary catalyst [21].

Assisting with preceding concerning matters it is transparently visible that environment has also effective consequence on human being. The extreme essence from resources and extensive birth in a moment has been captured as strong liable after a restless analyzation about the present plight of environmental plunder. Circumtancely the scientific communities become aware to see the exploitation on nature to discover the suitable alternatives of efficient catalyst towards synthesis of coenzyme, photochemical degradation and fossil fuels by minimizing the toxic effluents. In light of this, we have developed a new catalytics procedure for the synthesis of C3 substituted deoxy vitamers, bioactive intermediates substances, separation for the photogenerated electron-hole pairs and biodegradable-greener biodiesel by employing a greener, reusable, environmental friendly, non-toxic heterogeneous catalyst. To the best of our knowledge, this is the first report, demonstrates the mechanism in a novel way. We attempt to enlighten the properties how biocompatible eggshell related inorganic supported heterogeneous catalysis is bloomed in this field. Supported metal oxide was explored as a promising material in the organic synthesis and industrialization application [22–24].

Herein, we report biocompatible eggshell related inorganic supported heterogeneous catalysis, for the first time synthesis of C3 substituted deoxy, 2-nor deoxy vitamers and propargylamine, photocatalytic degradation under light irradiation and green long chain nucleophilic substituted fatty acid. Mechanism is probed through theoretical calculation. Catalysis is highly responsive towards respective reactions due to their ability to heighten reactivity as well as selectivity that results in better yields under flexible reaction conditions. The catalyst including environmental concern is re-applicable and strongly impressive.

2. Experimental

Sigma Aldrich provided 3-methylisoquinoline and some chemicals. Alfa-Aesar, Acros, and JT baker supplied other reagents and high performance liquid chromatography (HPLC) grade solvents which needed no any further purification. The air and moisture sensitive reactions were carried with HPLC grade solvent under argon/nitrogen atmosphere. The two cycles oxygen free water (freeze-pump-thaw) used to the cation exchange chromatography and oxidation reaction. The thin-layer chromatography of glass plate indicator ALOX-25 UV254 and DURASIL-25 UV254 were used to monitor the reaction. Either UV light (254 nm), basic $KMnO_4$, DNP solution, Iodine vapour and ninhydrin spray distinguished the sport on TLC. The phosphorylated analogues were purified by exchange chromatography using Amberlite CG-50 (H+ form) and Dowex 50×8 (H^+ form). Bruker 121 MHz (Bruker 300 MHz NMR), NMR 300 MHz, NMR 400 MHz, and NMR 600 MHz spectrometers recorded the data of ^1H and ^{13}C NMR and ^{31}P spectra respectively. TMS and 85% H_3PO_4 used external reference, the d-solvent of DMSO-d6, $CDCl_3$, CD_3OD- d4 or D_2O were taken as a standard proton-solvent references (1H: $CDCl_3$: 7.26 ppm, D_2O: 4.79 ppm, DMSO-d6: 2.50 ppm; 13C: DMSO-d6: 40 ppm;). MALDI–TOF mass spectrometer preserved the record of Mass spectra. Geometry optimizations were performed in gas phase at the b3lyp level with 6–31G(d,p) basis set. Sample morphology was obtained by field emission scanning electron microscopy (FE-SEM, JEOL JSM-7000F). Characterized structures were recorded by an X-ray diffractometer (Rigaku D/Max- 2500) operating at 30 kV and 50 mA with Cu Kα (λ = 0.154 nm) radiation. UV spectra and photocatalytic activity were noted using a Shimatzu UV-2550 spectrophotometer.

2.1. Egg shell

White chicken eggshells were obtained after peeling the outer cover of boiled eggs. The egg shells were dried and crushed in a mortar and pestle to obtain white powder.

2.2. Preparation of TiO$_2$ NPs

Sol-gel-hydrothermal method was chosen for the synthesis of TiO$_2$ NPs. Firstly, 4.5 mL of TTIP was dissolved in 20.5 mL anhy. EtOH to make a homogeneous solution. In another beaker 25 mL of EtOH was mixed with 25 mL distilled water. Above ethanolic solution of TTIP was added dropwise into the aq. EtOH under vigorous stirring. Formation of white gel was observed during the addition of TTIP indicating the formation of Ti(OH)$_4$. In order to achieve complete hydrolysis of TTIP, the gel was stirred at RT for 4–5 h. Then the gel was transferred into a Teflon lined autoclave and heated at 120 °C for 10 h. The obtained material was centrifuged and washed with water, ethanol several times and dried at 100 °C for 10 h. White powder was obtained upon grinding the dried material which was used as catalyst in our experiments.

2.3. Eggshell decorated TiO$_2$

Egg shell and TiO$_2$ NPs were finely ground and mixed by motor-pestle using mechano-chemical method. The solid solution was calcined in a tubular furnace under static air conditions at 900 °C for 4 h @ 10 °C/min, to transform the calcium species in the shell into CaO particles (Cat-ET). The main constituent on the eggshell is CaCO$_3$ (95%), the expulsion of CO$_2$ leads to the formation of CaO on TiO$_2$. Similarly, TiO$_2$ and only egg shell were also calcined at 900 °C for 4 h. The obtained white powders were labelled as Cat-T and Cat-E respectively.

Preparation of CaO immobilized TiO$_2$: Egg shell 900 °C and TiO$_2$ NPs were mixed by motor-pestle using mechano-chemical method. The mixture was calcined in a tubular furnace under static air conditions at 900 °C for 4 h @ 10 °C/min. The powders were marked as Cat-CT.

2.4. Preparation of Ag^0@CaO/TiO$_2$

20 mg CaO immobilized TiO$_2$ immersed in aqueous solutions of silver nitrate (0.23 mmol) was stirred at room temperature for 12 h. The resulting mixture was filtrate washed and dried also named as Cat-ACT.

2.5. Preparation of 3-deoxy pyridoxine 7b

An ice-cooled suspension of NaBH$_4$-Cat-CT (113.5 mg, 3 mmol–33 mg) in dry ethanol (15 mL) under nitrogen atmosphere was stirred for a 15 min, followed by slow addition of ethanol solution of dimethyl 2-methyl-4,5-pyridinedicarboxylate (0.1 g, 0.5 mmol). The reaction mixture was allowed to stir at room temperature for 5 h. Mixture was stirred for 30 min upon addition of catalytic amount of silver nitrate afterwards it was filtrated and washed with ethanol. Solvent was removed under reduced pressure, and solid was recrystallized with dichloromethane, afforded desired product 0.07 g (92%). ^{1}H NMR (300 MHz, DMSO): δ = 2.43 (s, 3H, 2-Me), 4.46 (s, 2H, 5′CH$_2$), 4.57 (s, 2H, 4′CH$_2$), 5.17 (b, 1H, 5′COH), 5.29 (b, 1H, 4′COH), 7.29 (s, 1H, 3-H), 8.28 (s, 1H, 6-H); ppm; 13C NMR (75.5 MHz, CD$_3$OD): δ = 23.9, 60.6, 61.4, 122.5, 132.6, 148.6, 152.2, 159.1 ppm; ^{13}C DEPT-135NMR (75.46 MHz, CD$_3$OD): δ = 148.4, 122.7, 61.5, 60.6, 23.9 ppm; MALDI–TOF MS: m/z = 154.07 (154.09 calcd for C$_8$H$_{11}$NO$_2$, M + H$^+$)

2.6. Compound 7a

Methyl 2-nor-4,5-pyridinedicarboxylate (0.1 g, 0.51 mmol), NaBH$_4$-eggshell/TiO$_2$ (113.5 mg, 3 mmol–33 mg) in dry ethanol (15 mL), under N$_2$ atmosphere, stirred at room temperature for 5 h. White solid, 0.06 g (92%); ^{1}H NMR (300 MHz, DMSO): δ = 4.51 (s, 2H, 5′CH$_2$), 4.60 (s, 2H, 4′CH$_2$), 7.43 (d, 1H, 3-H), 8.44 (s, 2H, 6-H,

2H); ppm; ^{13}C NMR (75.5 MHz, CD$_3$OD): δ = 58.5, 58.9, 120.4, 133.6, 147.8, 148.5, 149.2 ppm; MALDI–TOF MS: m/z = 140.06 (140.07 calcd for C$_7$H$_9$NO$_2$, M + H$^+$)

2.7. Preparation of 3-Deoxy pyridoxal oxime 9b

To a stirred solution of 2-Methyl-4,5-dihydroxymethylpyridine (0.5 g, 3.2 mmol) in dd water was slowly added to freshly prepared manganese dioxide at room temperature. The mixture was allowed to stir for 15 min, then occasionally addition of conc. H$_2$SO$_4$ was added to maintain the pH 3.5. After stirring for 4 h, unreacted manganese dioxide was filtered off then washed with minimum of water, [3-deoxy pyridoxal hemiacetal 8b: ^{1}H NMR (400 MHz, DMSO-d6): δ = 2.49 (s, 3H, 2-Me), 4.91 (d, 1H, J = 12.9 Hz, CH$_2$O), 5.06 (d,1H, J = 12.8 Hz, CH2O), 6.29 (d, J = 5.7 Hz, CH of hemiacetal form), 6.94 (d, J = 7.6 Hz, OH), 7.25 (s, 1H, 3-H), 8.46 (s, 1H, 6-H) ppm; 13C NMR (400 MHz, DMSO-d6): δ = 24.3, 69.3, 100.4, 117.4, 133.1, 142.9, 149.7, 157.1 ppm; ^{13}C DEPT-135NMR (75.46 MHz, DMSO-d6): δ = 24.3, 69.3, 100.3, 117.3, 142.8 ppm; MALDI–TOF MS: m/z = 152.08 (152.07 calcd for C$_8$H$_9$NO$_2$, M+H$^+$)] followed by addition of sodium acetate (401 mg, 4.8 mmol) and hydroxylamine hydrochloride (333.0 mg, 4.8 mmol). The solution was heated on steam-bath for 2 h and cooled to room temperature kept in refrigerator overnight. The desired product was isolated by filtration 55% (8b to 9b). ^{1}H NMR (300 MHz, DMSO-d6): δ = 2.46 (s, 3H, 2-Me), 4.59 (d, 2H, J = 4.4 Hz, CH$_2$O), 5.25 (s, 1H OH), 7.46 (s, 1H, 3-H), 8.34 (s, 1H, 6-H), 8.45 (s, 1H, 4′-CH), 11.76 (s, 1H, NOH) ppm; ^{13}C NMR (300 MHz, DMSO-d6): δ = 24.2, 59.5, 119.1, 131.7, 138.8, 146.2, 149.7, 157.4 ppm; MALDI–TOF MS: m/z = 167.10 (167.09 calcd for C$_8$H$_{10}$N$_2$O$_2$, M + H$^+$).

2.8. Compound 9a

The mixture of compound 7a (0.5 g, 3.5 mmol), manganese dioxide in dd water was stirred for 15 min, then maintain the pH 3.5 by occasionally addition of conc. H2SO4. After stirring for 4 h unreacted manganese dioxide was filtered off. [2-nor-3-deoxy pyridoxal hemiacetal 8a: ^{1}H NMR (300 MHz, DMSO) δ = 4.95 (d, 1H, J = 13.4 Hz, CHO), 5.10 (d,1H, J = 12.4 Hz, CH$_2$O), 6.33 (d, J = 7.8 Hz, CH of hemiacetal form), 6.96 (d, J = 7.6 Hz, OH), 7.45 (d, 1H, 3-H), 8.52 (d, 2H, 2-H &6-H) ppm; ^{13}C NMR (300 MHz, DMSO): δ = 69.0, 100.0, 117.9, 135.5, 143.4, 148.2, 148.4 ppm; MALDI–TOF MS: m/z = 138.05 (138.05 calcd for C$_7$H$_7$NO$_2$, M + H$^+$)] Sodium acetate monohydrate (434 mg, 5.3 mmol), hydroxylamine hydrochloride (368.2 mg, 5.3 mmol) was added stir at 100 °C for 90 min. The filtrated solid 55% (8a to 9b); ^{1}H NMR (300 MHz, DMSO-d6): δ = 4.65 (d, 2H, J = 4.4 Hz, CH$_2$O), 5.36 (t, 1H OH), 7.60 (d, 1H, 3-H), 8.38 (s, 1H, 6-H), 8.49 (d, 1H, 2-H), 8.60 (s, 1H, 4′-CH), 11.85 (s, 1H, NOH) ppm; ^{13}C NMR (300 MHz, DMSO-d6) δ = 59.1, 119.5, 134.1, 138.1, 145.6, 148.7, 149.7 ppm; MALDI–TOF MS: m/z = 153.07 (153.06 calcd for C$_7$H$_8$N$_2$O$_2$, M + H$^+$).

2.9. Compound 9c

^{1}H NMR (400 MHz, DMSO-d6): δ = 2.37 (s, 3H, 2-Me), 4.57 (d, J = 4.8 Hz, 1H, CH2OH), 5.31 (t, J = 5.1 Hz, 1H), 7.94 (s, 1H, 4′-CH), 8.57 (s, 1H, 6-H), 10.64 (s, 1H, OH), 12.16 (s, 1H, NOH) ppm; ^{13}C NMR (100 MHz, CDCl3) δ = 19.3, 59.2, 120.2, 132.7, 139.4, 147.2, 148.6, 150.2 ppm; MALDI–TOF MS: m/z = 183.08 (183.09 calcd for C8H10N2O3, M + H +).

2.10. Compound 8e

^{1}H NMR (400 MHz, DMSO-d6): δ = 2.36 (s, 3H, Ar-Me), 2.42 (s, 3H, 2-Me), 4.76 (s, 2H, 5′-CH2-), 5.46 (s, 5″-OH), 7.32- 7.41 (m, 4H, −C$_6$H$_4$-), 7.96 (s, 1H, H6), 9.17 (s, 1H, H4′) ppm; ^{13}C NMR

(100 MHz, CDCl3) δ = 18.3, 20.2, 59.1, 120.3, 121.5, 130.1, 137.8, 138.3, 145.4, 160.4 ppm; MALDI–TOF MS: m/z = 257.13 (257.11 calcd for $C_{15}H_{16}N_2O_2$, M + H$^+$).

2.11. Three-component coupling reaction

A mixture of aldehyde (1.0 mmol), amine (1.2 mmol), alkyne (1.5 mmol), and Cat-ACT (25 mg) was stirred with toluene at 100 °C for 24 h under argon atmosphere. After the completion of the reaction, column chromatography was used to purify the product using n-hexane/EtOAc to give the desired product in quantitative yield.

2.12. Procedure for the photo-degradation of MB

Experiments were carried out in a pyrex round bottom flask containing catalyst (Cat-CT) and methylene blue capacity of pollutant can improve the photocatalysis, leading to faster degradation of pollutant. So, MB degradation is the photocatalytic degradation of MB and sulphur site in the MB is sensitive to the calcium sites on these materials surface. Previous reports indicated that the pollutant adsorption on the catalyst surface plays a vital role which improves the efficacy of photons during the photocatalytic process as the adsorption aqueous solution. 20 mg of the catalysts were suspended in a 100-mL aqueous solution of 10 mg/L methylene blue (MB), then the suspension was stirred in dark for 30 min to attain adsorption-desorption equilibrium and then irradiated with a 25 W medium pressure mercury lamp. The concentration of photocatalyst was 0.2 g/L. The concentration of methylene blue in the solution was determined using the Lambda 950 UV–vis spectrophotometer by collecting the absorbance of MB at 664 nm.

2.13. Procedure for the preparation of biodiesel

100 mL 2-necked RBF was charged with 1 mL waste oil, 15 mL MeOH and 100 mg catalyst and carried out the reaction at 65 °C for 2 h under continuous stirring. After 2 h, the reaction mixture was kept stationary overnight for the clear separation of biodiesel and glycerol. The supernatant was and analysed by ^{1}H NMR with CDCl$_3$ as solvent.

The% conversion of methyl esters was calculated by using C = 100*2AME/3AαCH2 Where C = percentage conversion of triglycerides to methyl esters, AME = integration value of the methoxy protons of the methyl esters and Aα–CH2 = integration value of the α-methylene protons.

3. Results and discussions

3.1. Characterization of catalysts

X-ray diffraction pattern of ground eggshell powder showed similar peak pattern of calcite which is a crystalline mineral phase and thermodynamically stable polymorph of CaCO$_3$. XRD cannot detect noncrystalline organic biomaterials which is a characteristic of organic membrane on the eggshell. Solid calcium oxide or lime (CaO) was formed upon heating the calcite (CaCO$_3$) at elevated temperature 900 °C by the expulsion of CO$_2$. The peaks appeared at 2θ angles 32.36°, 37.50°, 54.00°, 64.30°, 67.48° were the characteristics of CaO consistent with an earlier report [25]. In addition, data also shows lower diffraction pattern of CaCO$_3$ and minor intensity of Ca(OH)$_2$ which can be formed trace interplay of CaO with water vapour on the air. The diffraction peaks of the CaO and TiO$_2$ phases were clear, indicating that Ca and Ti were present in the form of lime, anatase and rutile crystallites, respectively it shows in Fig. 2A. On the other hand, biomass components supported reduced silver zero catalysts showed characteristic peaks at 38.07, 44.29, 64.40, 77.44 (Fig. S1). The Raman peaks at wavenumbers of about
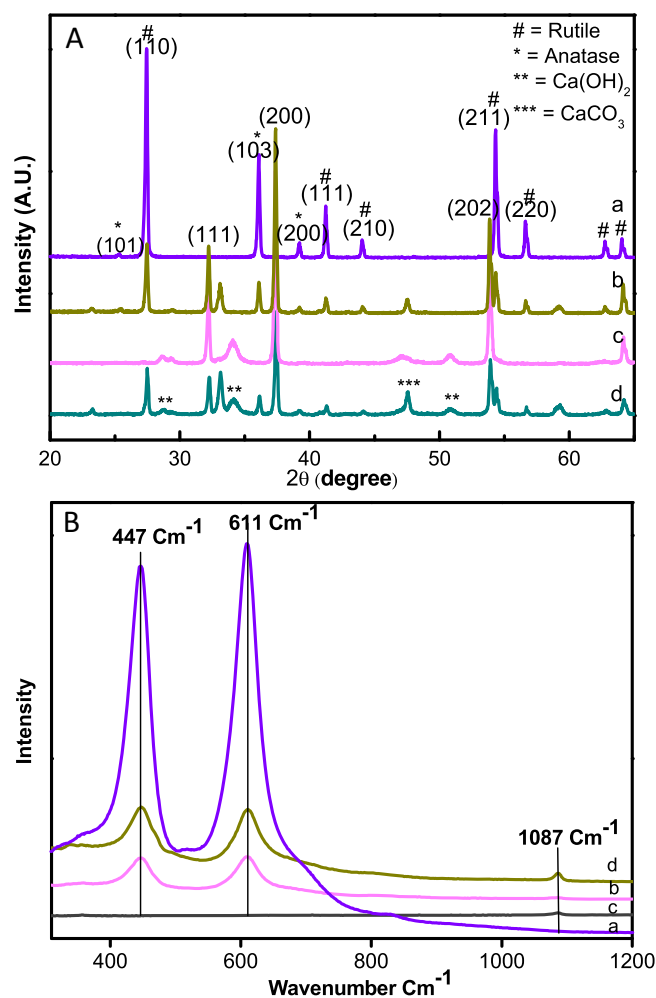
Fig. 2. XRD (A) and Raman (B) Picks of catalysts (a) Cat-T, (b) Cat-CT, (c) Cat-E (d) Cat-ET.

144, 196, 387, 514 and 633 cm^{-1} can be assigned to the anatase phase [26]. The typical peaks of the rutile phase are observed at 447, 611 cm^{-1}, which is attributed to no anatase phase when the material is calcined at 900 °C and some defect observed towards calcium side close to 1087 cm^{-1} (Fig. 2B). Fig. 3 depicts the result of Scanning electron micrographs were recorded for the calcined samples to observe the morphology. Eggshell possesses irregular crystal structure with high macroporisity and size of the particles is reduced and became more regular after the calcinations at 900 °C for 2 h. Agglomeration of the small particles can be observed with a size of 100–150 nm on respectively. The elemental analysis of the synthesized catalysts was performed by Energy dispersive respectively (Fig. S2). The XPS spectra of calcinated samples of respective catalysts are shown in Fig. 4A. Fig. 4E exhibits two peaks at 346.4 and 349.9 eV, corresponding to the binding energy of Ca2p$_{3/2}$ and Ca2p$_{1/2}$, respectively. A single feature at 531 eV corresponds to the O1s spectra of lattice O2$^-$ in CaO (Fig. 4D). In case of TiO$_2$, two peaks were observed at 464.0 and 458.1 eV, which is equivalent to Ti 2p$_{1/2}$ and Ti 2p$_{3/2}$ (Fig. 4C). The peak separation of 6 eV between the Ti 2p$_{1/2}$ and Ti 2p$_{3/2}$ signals is in good agreement with the earlier reports [27]. The O1s spectra of lattice O2$^-$ in TiO$_2$ was observed to be at 530 eV. However, from the XPS survey spectrum of Cat-CT sample, it can be observed that the sample includes Ti, O, C, and Ca elements. The C element can be ascribed to the residual carbon from precursor solution and the advention hydrocarbon from XPS instrument itself. Ti2p$_{1/2}$, Ti2p$_{3/2}$ peaks were observed at 464, 458 eV and Ca2p$_{3/2}$ and Ca 2p$_{1/2}$ peaks were observed at
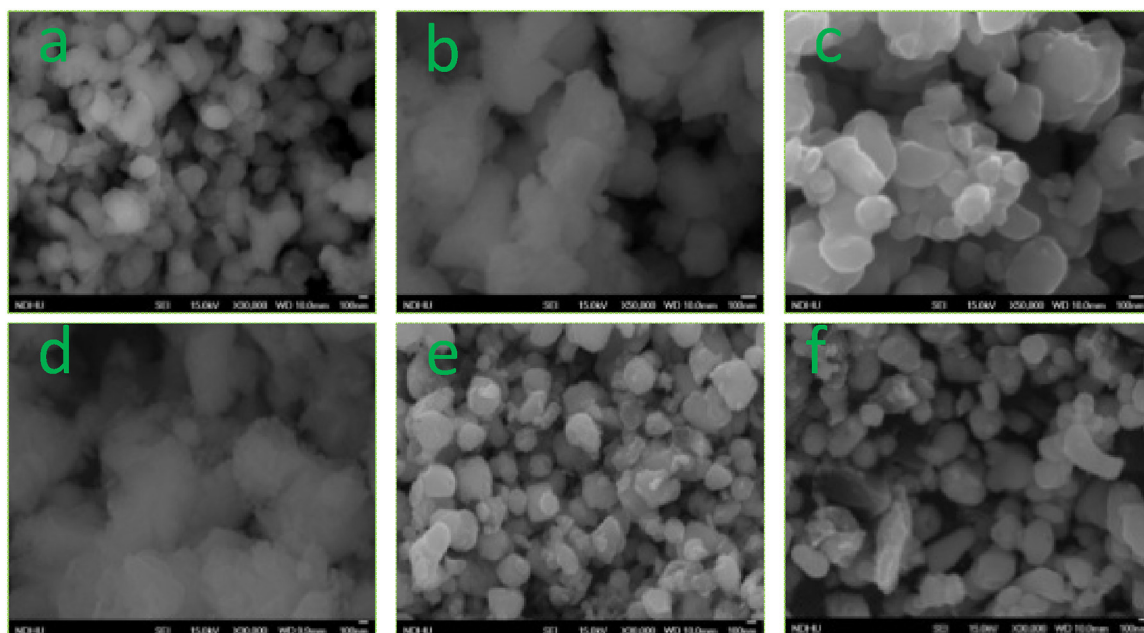
Fig. 3. SEM images of (a) Cat-ET, (b) Cat-E, (c) Cat-T, (d) Cat-CT, (e) Cat-ACT, (f) Cat-ACT after reaction.

346.4, 349.9 eV. The shift in the binding energies of Ca and Ti indicate the formation of Ca/Ti composite. Fig. 4B shows two peaks at 368 and 374 eV due to Ag $3d_{5/2}$ and Ag $3d_{3/2}$ orbitals respectively, which designates that the silver atoms present in the $Ag^{(0)}$, these results are consistent with previous reports [28]. The UV–vis absorption spectra of inorganic supported composite nanoparticles are depicted in Figure- S3. The sample Cat-E and Cat-ET showed similar type of absorption properties, whereas Cat-CT showed different absorbance. The estimated band gap energy for the Cat-CT and Cat-T are 2.75 and 2.82 eV respectively (Fig. 4G). This may be due to defects on the CaO surface, some of Ca^{2+} ions enter in the lattice substituting Ti^{4+} and inducing oxygen vacancies which decreases the band gap [29]. From nitrogen adsorption-desorption were quantities surface area as well as porosities of respective catalysts exhibited both macroporous and mesoporous structures (Fig. 5).

3.2. C3 pyridoxal-5′-phosphate analogues

The synthetic routes of 3-deoxy substituted pyridoxine, 1-deaza pyridoxine and other derivatives are depicted in Scheme 1. The core of pyridine and benzene dicarboxylic acid was obtained by oxidation of aza-aromatics compound using O_3 oxidation. For obtaining better result in case of pyridine dicarboxylic acid a considerable drop of water was mingled time to time. Therefore, concern of pyridine nucleotide, esterification with Jones et al. [30] method has also greatest extent towards the reaction. Our group and Blackwood et al. [31] were able to achieve less than 8% diester due to slow rate reactivity, dicarboxylic ester yield of 54%, using concentrated sulfuric acid in methanol at reflux condition. Then reduction with lithium aluminium hydride in different polar aprotic solvent was not encouraging by yield due to over extensive decomposition, which resulted the formation of different analogues of monomethyl ester, unwanted quantitative products. Solvent extraction from water is also challenging. In order to improve the reactivity as well as, selectivity, we have resolved the saturated workup using potassium carbonate/acetone by introducing new approaches, using environment friendly heterogeneous catalysis. The series of reactions were tested with polar protic solvents and checked their activities. Blank experiments were performed using only $NaBH_4$,

Cat-T or Cat-ET, no progress in the reaction was observed on all the catalysts. The reaction was optimized by using various catalysts in various solvents. Though, the reaction was progressed in the case of $NaBH_4$/Cat-T and $NaBH_4$/Cat-E, but the conversion was low. Interestingly, two fold conversions were achieved on $NaBH_4$/Cat-ET and better yield on $NaBH_4$/Cat-CT. However in polar protic solvent like ethanol, desired product was obtained with excellent yield as depicted in Table 1 entry 8. The progress of the reaction was not seen using different polar aprotic and non-polar solvents such as DMF, THF, pentane and DCM respectively (Table 1, entries 10–15). It is also significant that in our current method, we have not observed any by products like monomethyl ester, etc. All the experiments were exploited to the Table 1 entry 8. The reaction was checked by TLC, isolation recrystallization and characterization was done by NMR spectroscopy. From proton NMR (see supporting information) the synthesized product 7b produced two singlets near weak field at 8.28, 7.29 in 1:1 ratios recognized as a pyridine proton. In deuterated dimethyl sulfox-

Table 1
Optimized reaction condition of 3-deoxy pyridoxine derivatives[a] (4,5 −dicarboxylic esters of 6 → 3-deoxy pyridoxine).

Entry	Catalyst with NaBH4	Solvent	Time (h)	Temp	Yield[b] (%)
1	–	C_2H_5OH	12 h	Reflux	NR
2	$NaBH_4$ [c,d]	C_2H_5OH	12 h	Reflux	NR
3	Cat-E [d]	C_2H_5OH	12 h	Reflux	NR
4	Cat-T [d]	C_2H_5OH	12 h	Reflux	NR
5	Cat-E	C_2H_5OH	8 h	RT	60
6	Cat-T	C_2H_5OH	7 h	RT	45
7	Cat-ET	C_2H_5OH	5 h	RT	82
8	Cat-CT	C_2H_5OH	5 h	RT	92
9	Cat-CT	CH_3OH	7 h	RT	85
10	Cat-CT	C_5H_{12}	12 h	RT	NR
11	Cat-CT	C_6H_{14}	12 h	RT	NR
12	Cat-CT	CH_2Cl_2	12 h	RT	NR
13	Cat-CT	CH_3CN	12 h	RT	NR
14	Cat-CT	THF	12 h	RT	NR
15	Cat-CT	$(C_2H_5)_2O$	12 h	RT	NR

[a] Reaction condition: Pyridine dicarboxylic ester (0.5 mmol), Catalyst (33 mg).
[b] Isolated yield.
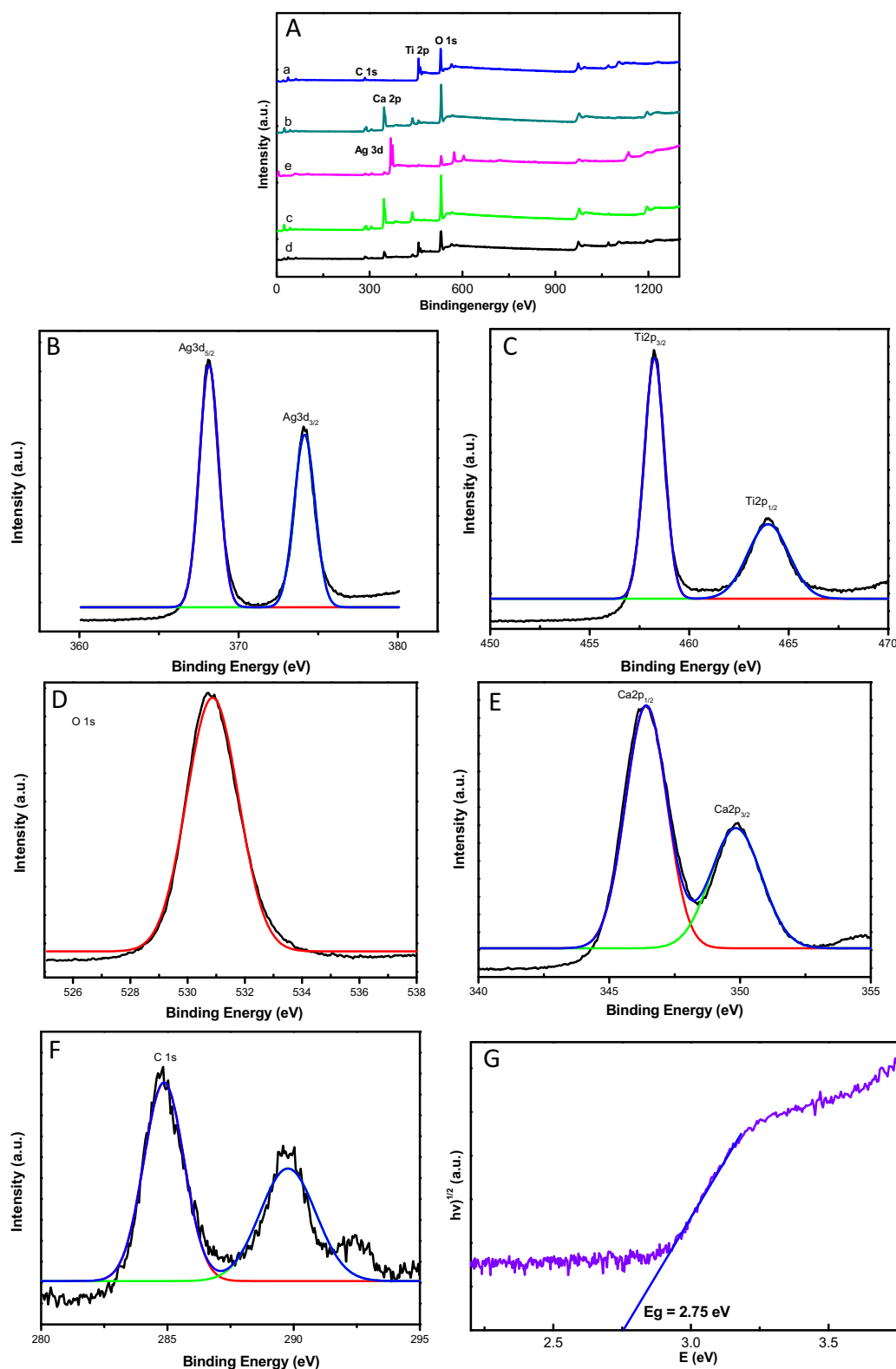[c] Without Catalyst.
[d] without $NaBH_4$.

Fig. 4. (A-F) XPS spectra of respective catalysts (a) Cat-T, (b) Cat-CT, (c) Cat-E, (d) Cat-ET, (e) Cat-ACT and (4G) band gap of Cat-CT.

ide solvent, two broad singlets at 5.29, 5.08 ppm were typically for 4′COH, 5′COH hydroxyl proton but in d-methanol, it was not observed because of the exchange of proton. Two singlets at 4.57, 4.46 ppm with a 1:1 ratio were also identified two protons for 4′CH$_2$ and 5′CH$_2$ respectively. From ^{13}C NMR and ^{13}C DEPT-135 NMR in deuterated methanol, peak at 159.0, 152.1, and 132.6 defined three

quaternary carbons in pyridine ring and at 148.6, 122.5, 61.4, 60.6, 23.9 ppm gave all CH and CH$_3$ in a phase and opposite to CH$_2$ carbon peaks respectively, from MALDI–TOF MS: m/z = 154.05 (154.08 calcd for C$_8$H$_{11}$NO$_2$, M + H$^+$). After optimization, we conducted same reactions with diverse 4,5 – dicarboxylic esters substituted pyridine nucleotide at room temperature, such as Me, Et, Pr, iPr,
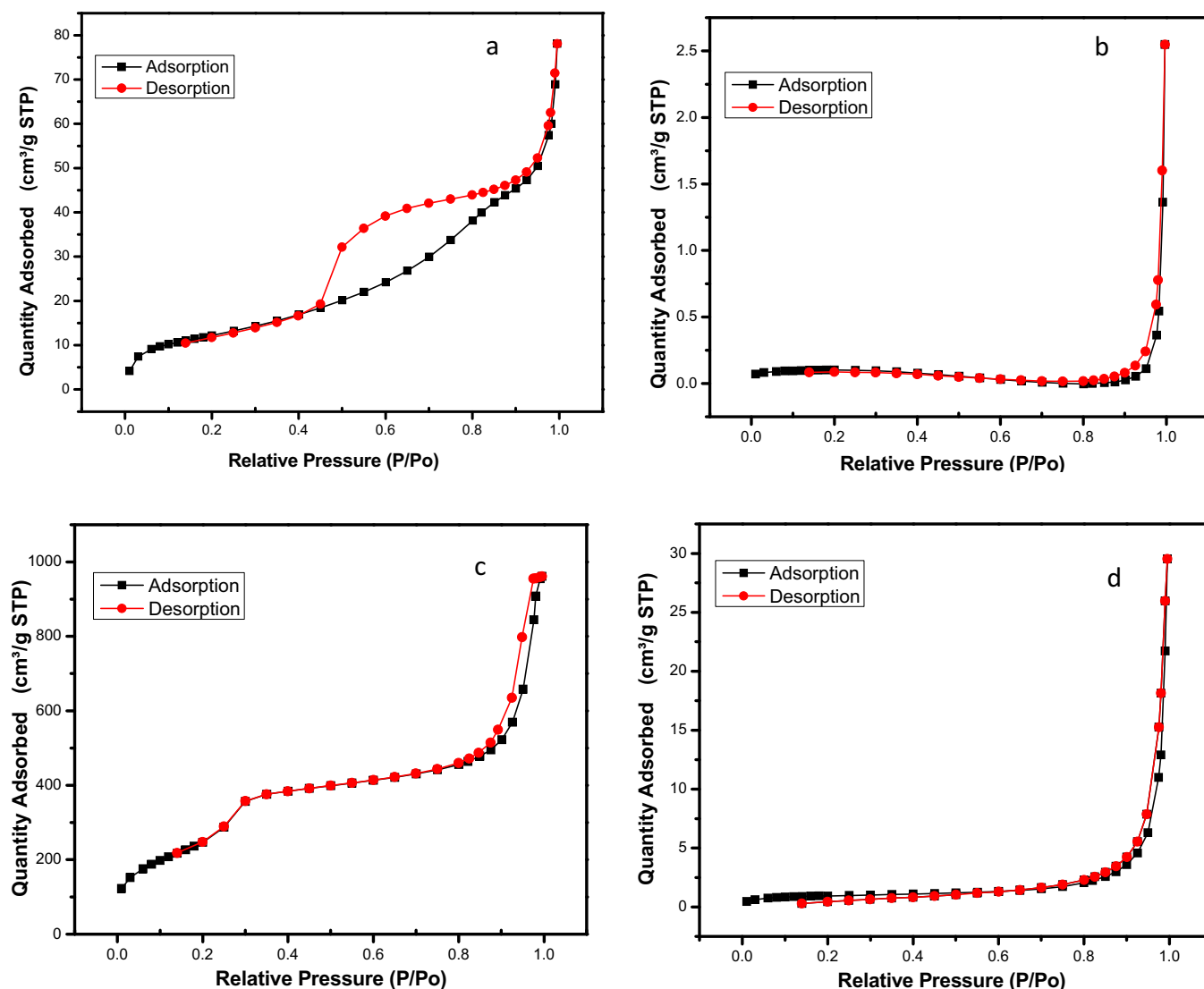
Fig. 5. Nitrogen adsorption–desorption isotherm of respective catalysts (a) Cat-E, (b) Cat-T, (c) Cat-ACT, (d) Cat-CT.

Table 2
Synthesis of 3-deoxy pyridoxine derivatives (4,5 —dicarboxylic esters of 6 → 3-deoxy pyridoxine).

Entry	R_1	R_3	Time (h)	Yield[b] (%)
1	H	H	12 h	NR
2	H	CH_3	5 h	92(7a)
3	H	CH_3CH_2	5 h	91(7a)
4	H	$CH_3CH_2CH_2$	8 h	86(7a)
5	H	CH_3CHCH_3	12 h	76(7a)
6	H	$CH_3CH_2CH_2CH_2$	12 h	~74(7a)
7	CH_3	H	12 h	NR
8	CH_3	CH_3	5 h	92(7b)
9	CH_3	CH_3CH_2	5 h	90(7b)
10	CH_3	$CH_3CH_2CH_2$	8 h	86(7b)
11	CH_3	CH_3CHCH_3	12 h	75(7b)
12	CH_3	$CH_3CH_2CH_2CH_2$	12 h	72(7b)
13	H	H	12 h	NR
14	H	CH_3	1 h	NR
16	CH_3	H	12 h	NR
17	CH_3	CH_3	12 h	NR

13–17 Benzene moiety.

[b] Isolated yield, NR: No reaction.

and nBu moiety which was afforded desired products in good yields (Table 2). From the steps involved in the mechanism, the reduction reaction requires hydride transfer from the donor, BH_4^-

ion. Under the current experimental conditions in the presence of $NaBH_4$/Cat-CT, chemisorption of BH_4^- happens on the surface of the catalysis followed by discharge of electrons from BH_4^- through Cat-CT with good yields. From the steps involved in the mechanism, the reduction reaction requires hydride transfer from the donor acceptor. Ti^{4+} and Ca^{2+} active centres are surrounded by BH_4^- ions with high electrostatic interaction M^{n+} (M = Ca, Ti) which causes an easier removal of H^- ions. In addition carbonyl oxygen and pyridine nitrogen coordinated with the catalyst surface increase electrophilicity of carbonyl carbon which leads to contribute considerable hydrides ion attraction. On the other hand electron cloud polarization towards electron-sink is more predominant compare to carbonyl oxygen Lewis adduct as we observe with benzene moiety, there was no reduction (Table 2, entries 13–17). In addition inducing oxygen vacancies also play major role to generate hydride ion which is favorable for the formation of the products. The polar protic solvent offers the required H^+ ions for the completion of the reduction reaction, whereas polar aprotic and non-polar solvent medium doesn't progress the reaction which is in accordance with our results in Scheme S1a. In the next step, selective oxidation followed by schiff bases with aromatic amines is one of the most suitable steps in order to extract substituted pyridoxal-5′-phosphate analogues. As per our observation and literature studies fabricate formation of schiff base of pyridoxal analog appears to
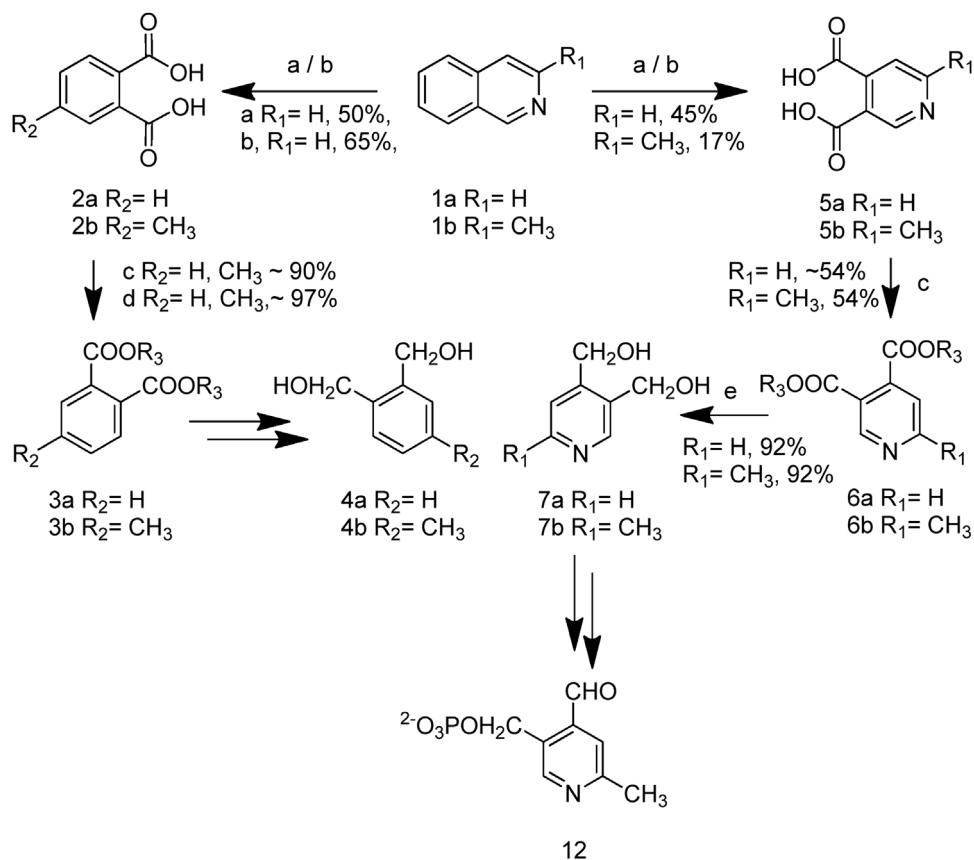
Scheme 1. Reagents and conditions: (a) excess ozone, acetic acid, water, RT; (b) potassium permanganate; water (c) conc. H_2SO_4, MeOH/EtOH, reflux, 2days; (d) dimethyl carbonate, conc. H_2SO_4, 85 °C, 6 h (e) NaBH$_4$, Cat-CT, EtOH.

be pliable showed in Scheme 2. Therefore we have put much effort to make schiff base at the 4′ position of 3-deoxyPL with aromatic amine but problems were encountered in the straight synthesis under these conditions. Schiff bases of 3-deoxypyridoxal with p-anisidine/p-toluidine could not be obtained. Similar kind of reaction was tried with 3-O-Methylpyridoxal and same results
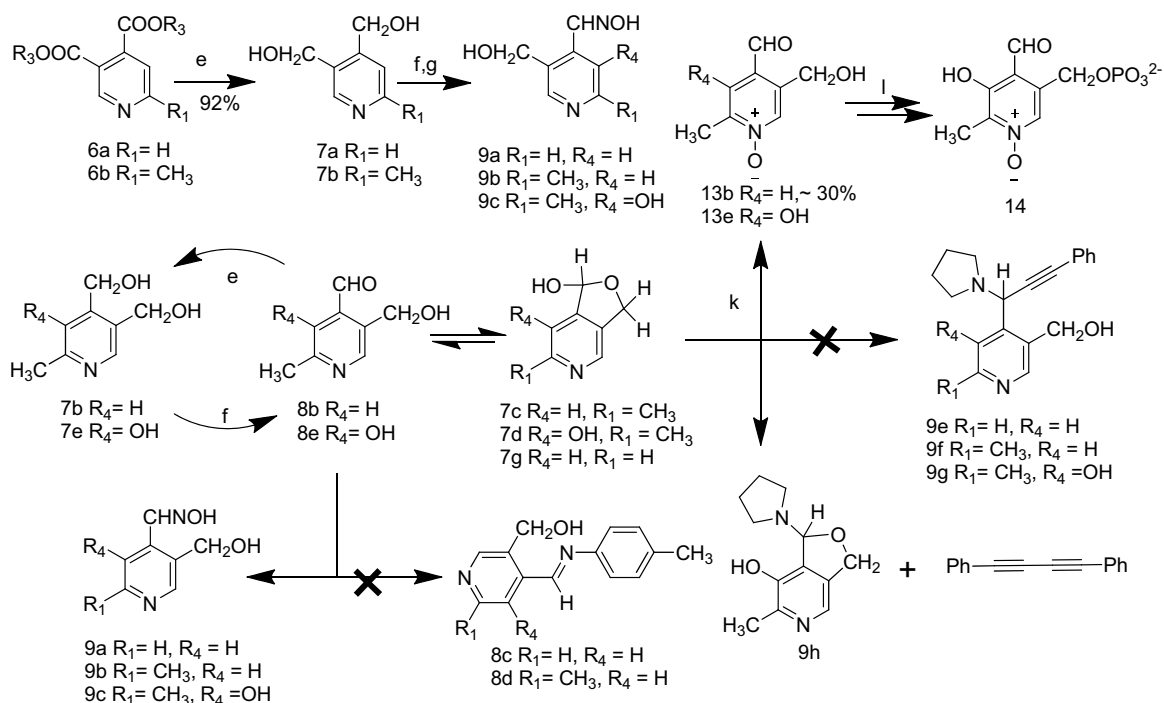
Scheme 2. Reagents and conditions: (e) NaBH$_4$, Cat-CT, EtOH; (f) MnO$_2$, H+, H$_2$O; (g) NH$_2$OH HCl/p-toluidine, NaOAc, H$_2$O; (k) mCPBA, THF, 0 °C; (l) Our group [10].
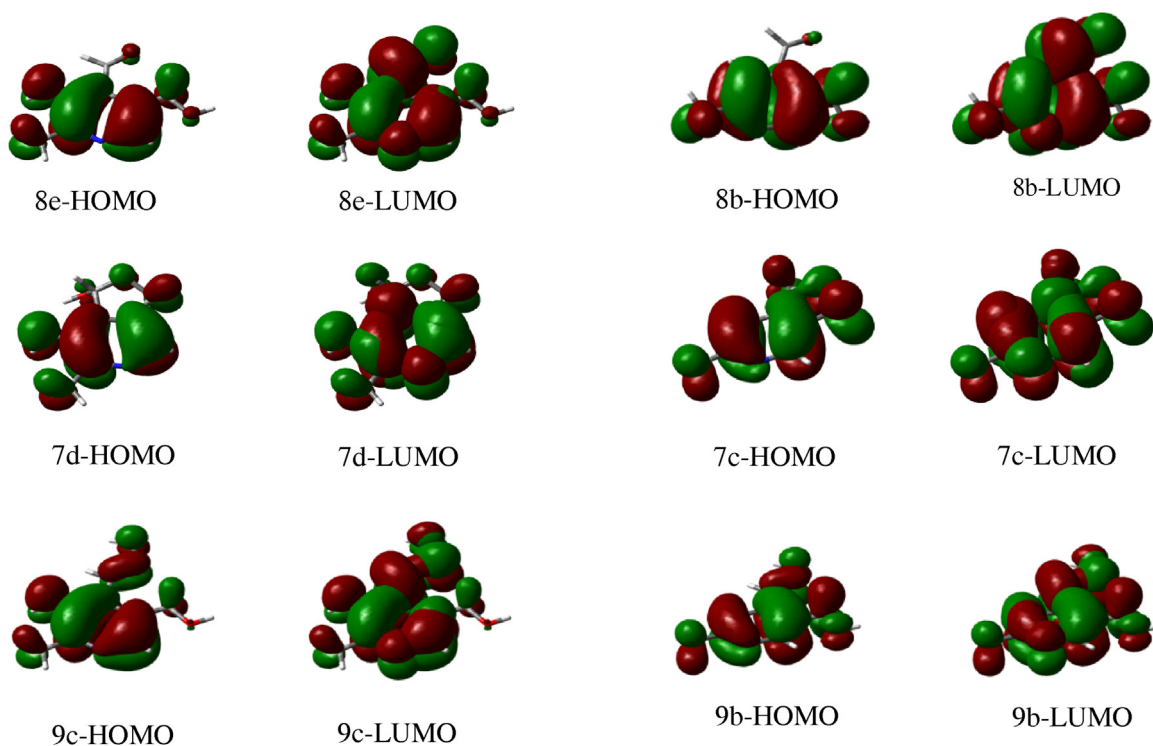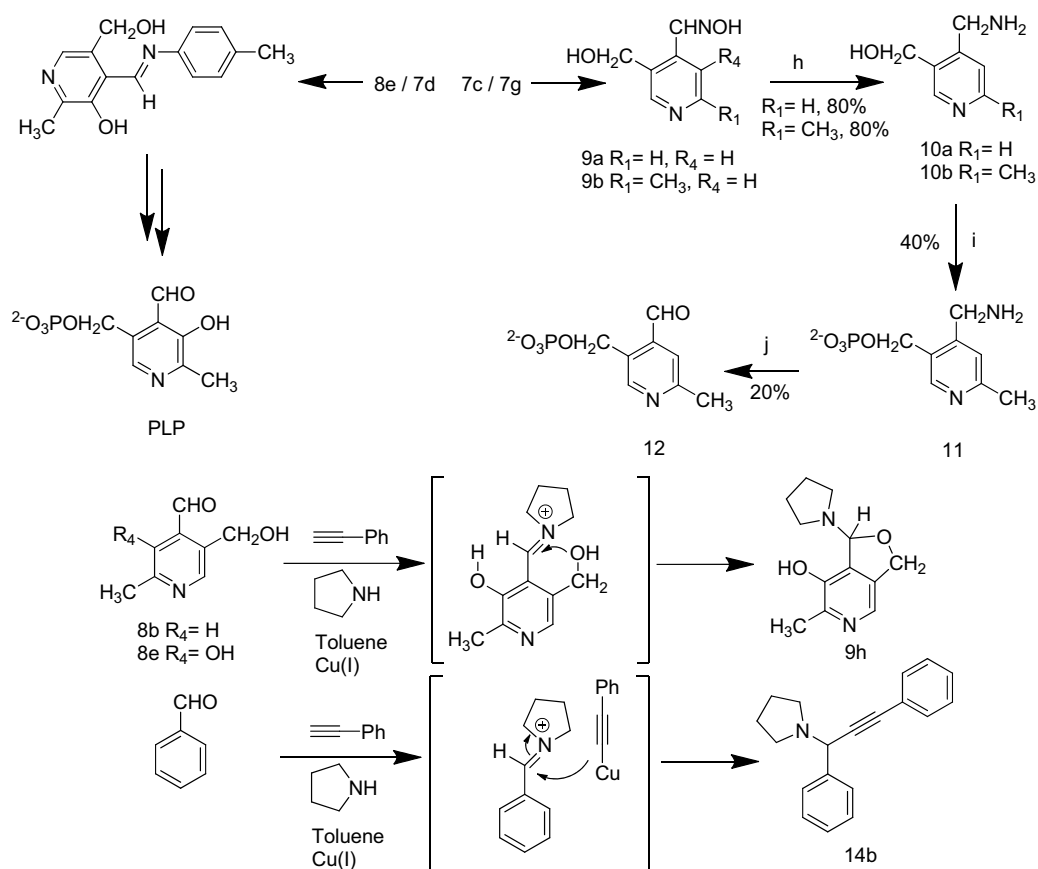
Fig. 6. Surface plots of the highest and lowest singly occupied molecular orbitals of respective organic molecules.

Scheme 3. Reagents and conditions: (h) Pd/C (10%), CH_3OH; (i) P_2O_5 & H_3PO_4, HCl, EtOH, ether, aqueous NH_3; (j) HC(O)COONa H_2O, acetic acid, Cupric acetate.
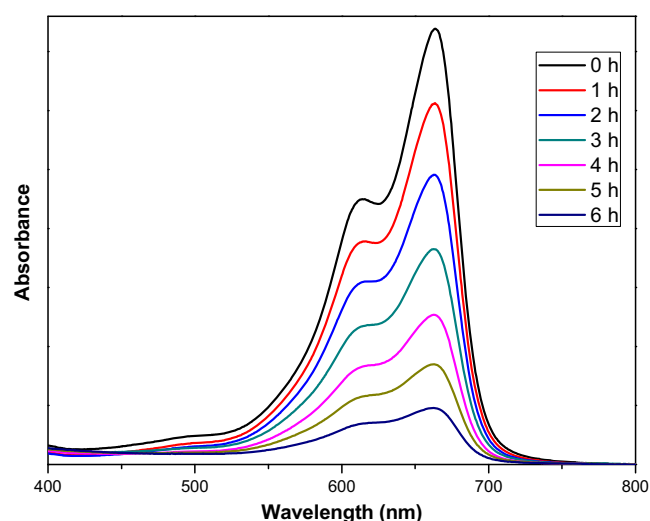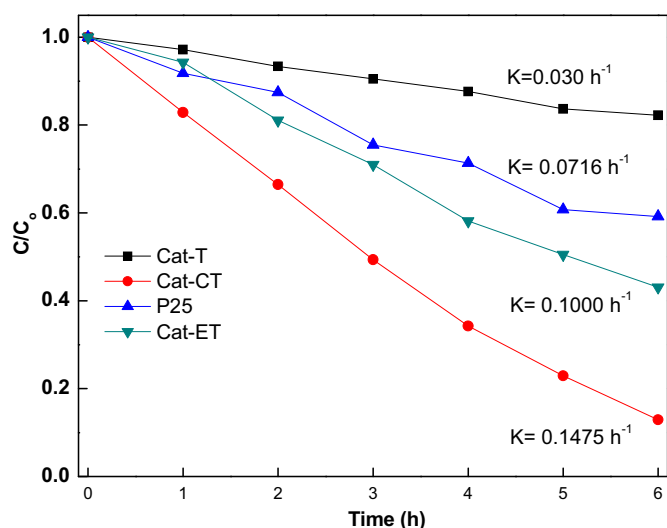
Fig. 7. Spectral changes upon the time C/C_0 degradation of MB.

Table 3
Optimized reaction condition of propargylamine 14b derivatives (3-component coupling of Benzaldehyde, piperidine, and phenylacetylene).
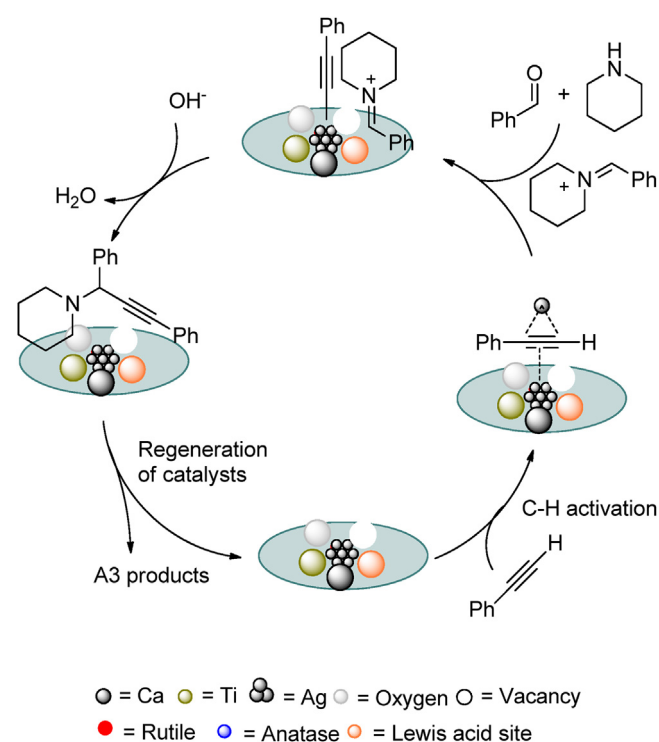
Entry	Catalyst	Solvent	Time (h)	Temp	Yield[b] (%)
1	Cat-ACT	H_2O	24 h	100	–
2	Cat-ACT	DMF	24 h	100	Traces
3	Cat-ACT	DMSO	24 h	80	Traces
4	Cat-ACT	C_2H_5OH	24 h	80	40
5	Cat-ACT	Dioxane	24 h	101	Traces
6	Cat-ACT	CH_3CN	24 h	80	62
7	Cat-ACT	CH_2Cl_2	24 h	35	Traces
8	Cat-ACT	Toluene	24 h	100	91
9	Cat-CT	Toluene	24 h	100	Traces

[a] Reaction condition: Benzaldehyde (1 mmol), piperidine (1.2 mmol) and phenylacetylene (1.5 mmol), Catalyst (25 mg).
[b] Isolated yield.

Furthermore, pyridoxal of 8b, 8e treatment with Cat-CT in ethanol: water (5:1) at room temperature affords the resultant product 7b, 7e in good yield respectively (Scheme 2). The reactivity of pyridoxal was checked using A3 coupling condition9a but unfortunately we did not observe any three component products which may be due to the 5′ hydroxyethyl group, a trace amount of 9 g and qualitative amount diphenylbutadiyne was obtained (Scheme 3). The hydroxyl group replaced by hydrogen to form hemiacetal in qualitative yield that we have observed from NMR spectroscopy under acidic condition which indirectly support the formation of N-Oxide without protection of 4′ alcohol group as shown in Scheme 2.

were acquired. Phenolic hydroxyl group take part in intramolecular acid catalysis, our result shows some significant progress as Stambolieva and Co-workers [32] showed C3 free hydroxyl group leads to a decrease degree of hydration and hemiacetal of the 4′ aldehyde at C3 free hydroxyl group. Here we apply computational and experimental aspect to provide mechanistic insights into the nature of substituted vitamers. The basic structure was modified at position 3 with heteroatoms to hydrogen atom. The derived derivatives of hetero aromatics system showed intense activity. To understand the electrophilic and nucleophile behaviour of 3 deoxy compound motivated us to recognize molecular orbital property and optimized geometry (Fig. S5). The molecular orbital of respective molecule indicate that MO of P_Z, mostly localized into the two halves three centered neucliotide ring. However the lowest excited state MO is almost overlapping on the aromatic core and spread over the C-4′ fragment shown in Fig. 6. The hydroxyl group at 3-position was able to offer lower energy absorption increase the electron density at C4 carbon which also has been interpreted 2-nor methyl derivative Fig. S6. The C3 hydrogen substituted pyridoxal indicate absence of self-catalytic group decrease the electron spin delocalization from the π-system of pyridine ring nitrogen lone pair to the C-4′ of the carbonyl group. Stambolieva and Co-workers [32] showed C3 free hydroxyl group leads to a decrease degree of hydration and hemiacetal of the 4′ aldehyde at C3 free hydroxyl group. Considering the reactivity of pyridoxal (8b) with hydroxylamine in imine reaction, span the analogues of pyridoxal derivatives under optimized reaction conditions both the selective mono-phosphorylated desired products 11 and 12 were generated with good yields of 40% and 20% respectively depicted in Scheme 3.

Scheme 4. Mechanism of A³ coupling reaction.

14a R_2 = (-C$_4$H$_8$)   14b R_2 = (-C$_5$H$_{10}$)   14d R_2 = (-C$_6$H$_5$)

14c R_3 = (-CH$_3$)   14e R_3 = (-OCH$_3$)   14f R_4 = (-C$_6$H$_{11}$)

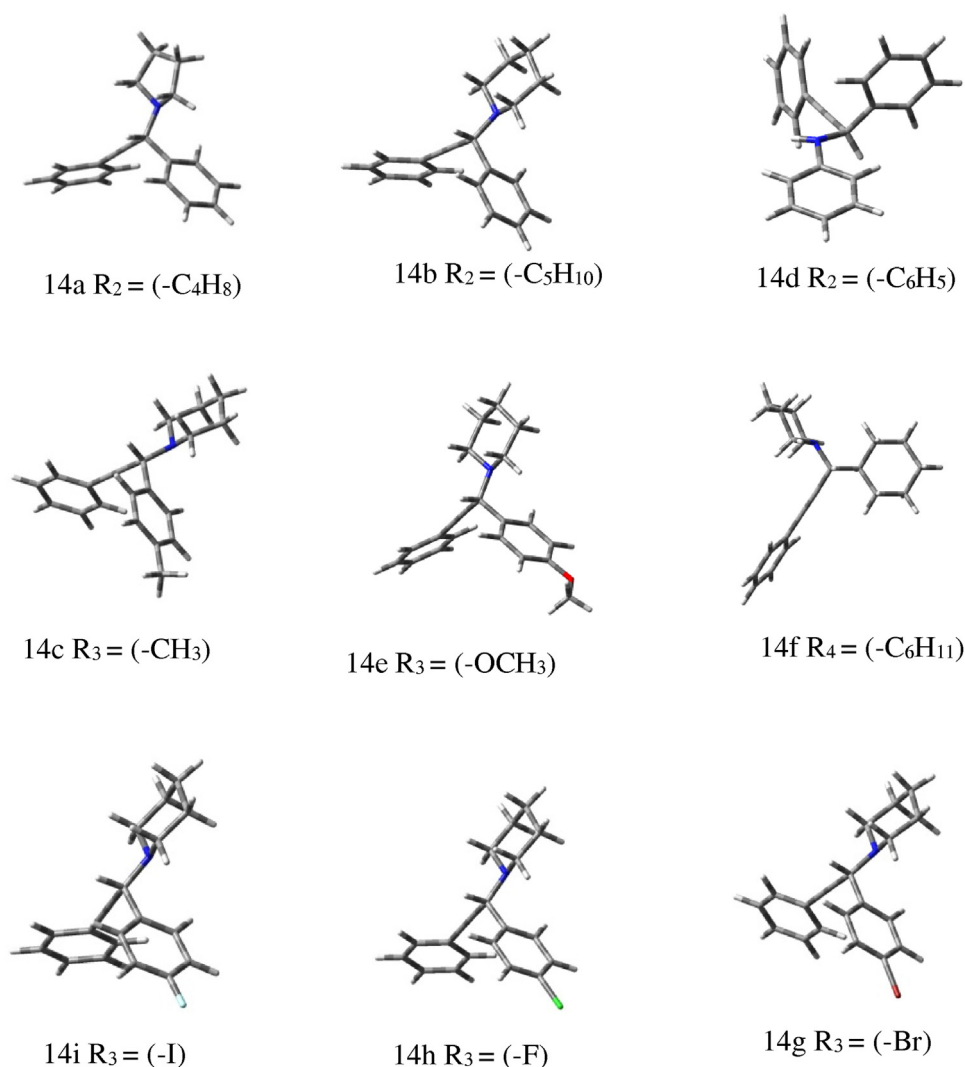14i R_3 = (-I)   14h R_3 = (-F)   14g R_3 = (-Br)

**Fig. 8.** Optimized structures (b3lyp/6–311 + +g(d,p) of A3 coupling products.

3.3. Photocatalytic activity

The photocatalytic accomplishment of the Cat-CT and Cat-ET composites were figure out by the degradation of environmental pollutants methylene blue (MB) under visible light irradiation. For comparison, degradation of MB on prepared catalysts based on eggshell derived composites displayed higher photocatalytic activity than TiO$_2$ and commercial P-25 TiO$_2$ powder with visible-light. Cat-CT exhibited photo degradation rate of 0.147 h^{-1} which is 4.9 times that of TiO$_2$, 2 times more than P25 and 1.4 times of Cat-ET respectively as shown in Fig. 7. The MB photocatalytic degradation and mechanistic representation of eggshell derived can be seen in Fig. S4.

3.4. Fatty acids esterification reaction

On the other hand long-chain nucleophilic substitution was the conclusive product of eggshell-derived catalysts after kept it in careful observation. Either eggshell or titanium oxide nanoparticle haven't showed any activity towards long-chain nucleophilic transesterification. Cat-CT exhibited of 97% yield, showed closer similar activity with Cat-C and Cat-ET with 94.5%, 95.7% yield respectively. This indicates presence of basic sites accelerated the transesterification due to electrostatic interaction between carbonyl oxygen and Ca^{2+}/Ti^{4+} ions, partial positive charge will be created on carbonyl oxygen of fatty acid ester which generates electrophilic centre on the carbonyl carbon atom. Methoxy group from the methanol will attack on the electrophilic centre to form fatty acid methyl ester and glycerol which is depicted in Scheme S1b. TiO$_2$/ZnO catalyst exhibited 92.2% of FAME conversion in 5 h at 60 °C using 200 mg catalyst loading [33], TiO$_2$/MgO showed 92.3% methyl ester at 120 °C for 6 h [34]. However, Cat-CT, sample exhibited better activity of 97% within 2 h at 60 °C as shown in Table S1. The formation of fatty acid methyl esters from cooking oil catalyzed by Cat-CT, Cat-ET and Cat-E was analysed using ^{1}H NMR (Supporting information). A singlet peak at 3.63 ppm and at 2.28 ppm was observed which can be attributed to methoxy protons and α-methylene protons respectively. Strong signal at 1.272 ppm arises from the methylene proton of carbon chain and a peak at 0.860 ppm arised due to terminal methyl protons. Reusability is one of the most essential assets for a heterogeneous catalyst. Reusability of the Cat-CT catalyst was examined for 4 cycles with 0.1 g by keeping a methanol to oil ratio of 15:1, a reaction temperature of reflux for 2 h. After each cycle, the solid catalyst was filtered off, washed with methanol to remove the adsorbed stains and dried for further use. The results indicate that a high biodiesel conversion of above 90% was achieved for all the 4 tested runs. For the fresh sample, the nucleophilic substituted biodiesel yield was 97%. After each reaction, the catalyst was separated, washed by methanol, and then dried for reuse.
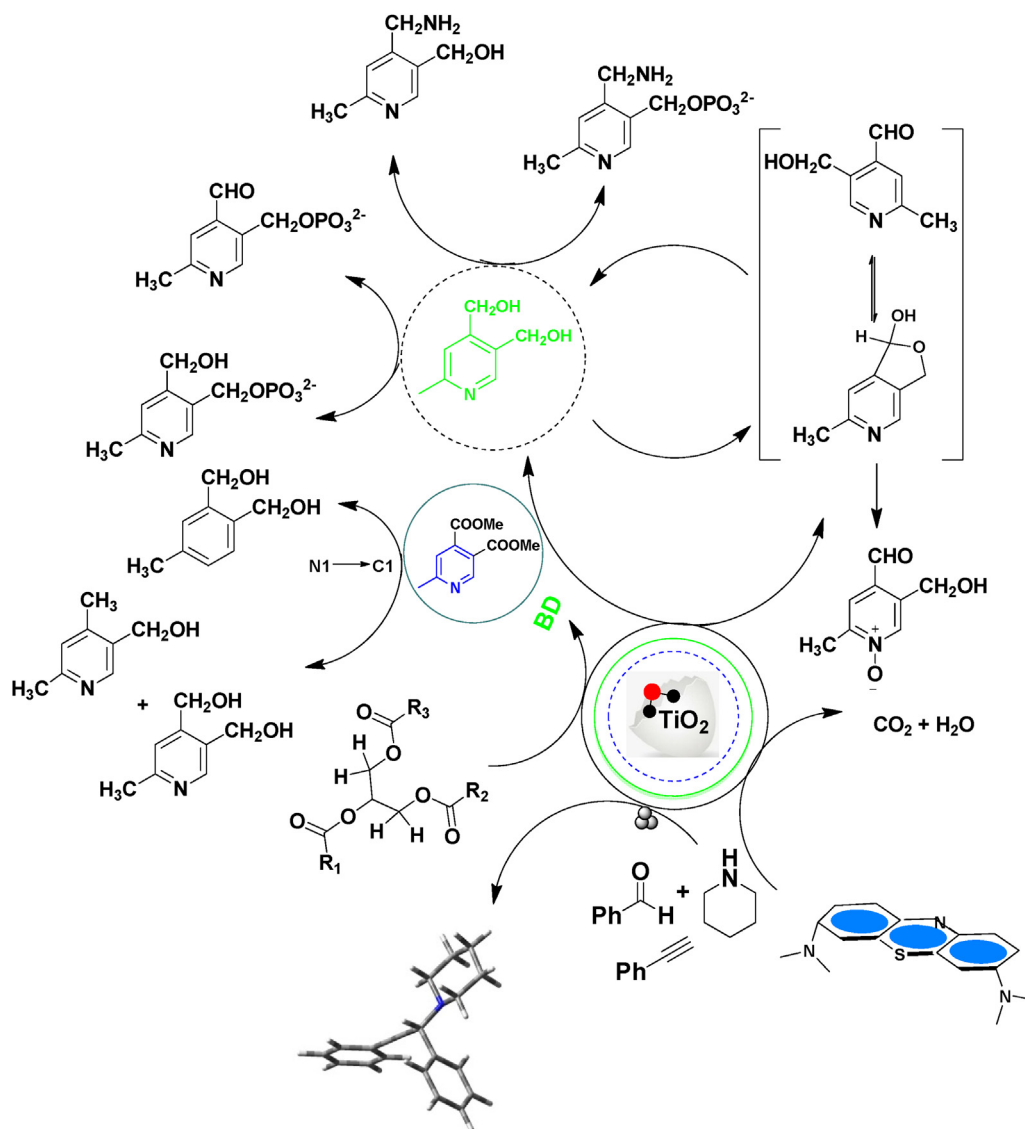
Scheme 5. Reaction Outline of eggshell supported catalysts.

3.5. C—C coupling reactions

A[3] coupling derivatives a versatile class of compounds have far extending impact in the various synthesis of heterocyclic bioactive compounds and natural products etc [35–38] represent in Fig. 1 (5–8). Some of coupling derivatives of propargylamines become assured to be potent antiapoptic agents that prevent neurons against death of cell in cellular and animal models of neurodegenerative disorders [39,40]. Potent molecule synthesized regular reaction condition with a strong base and organometallic reagents [41–43]. Where we introduced a green and highly efficient method has been developed for the synthesis of propargylamine in the presence of biocompatible eggshell supported inorganic smart probes Ag[(0)] (Cat-ACT). In our studies, benzaldehyde, amine source piperidine and alkyne of phenylacetylene in toluene were chosen as a model reaction and effective catalysts were examined to the model under optimizing conditions results are shown in Table 3. No reaction product was observed at room temperature even after 24 h of stirring. Significant amount reaction products were obtained in presence of heterogeneous catalyst under reflux condition. It indicates that the changing of the solvent and catalyst at ambient temperature influenced the desired three component coupling

products. The nanoparticle shows nice catalytic activity in non-polar organic solvent, but an important drop of desired product was observed when the solvent was changed to polar protic, polar aprotic this result is in agreement with Mallampati et al. [22]. To explore the scope of this reaction various type of A[3] component was examined. The optimal condition is found better yield. Optimized the structure with b3lyp/6–311++g(d,p) energy level using gaussian 09 Fig. 8. Based on our experimental results, the possible mechanism was proposed as shown in Scheme 4. Inorganic silver supported surface assisted electrostatic pi interaction with substituted acetylene to increase acidity of terminal proton. We speculate that formation of the corresponding silver probes supported acetylene intermediate structure. Acidic hydrogen might be attached to the surface oxygen or bridged oxygen of heterogeneous catalysts to form hydroxyl group which could be reopen intermediate to form RC_2^- acetylide anion [44]. As a consequence direct nucleophilic addition of carbon-nitrogen double bond of imine to produce corresponding propargylamine. This heterogeneous catalyst has numerous benefits to be used for further reaction.

Heterogeneous eggshell related metal supported catalysts advantageously have vast implication towards respective reaction shorten in Scheme 5.

4. Conclusions

In summary, we have reported for the first time highly efficient, greener and reactive CaO-TiO$_2$ heterogeneous catalyst. It has become enormous attention for smooth ability and promising flexibility to extend the scope of organic reaction and environmental concern. This catalyst was used to synthesize a wide variety of biologically active analogues and green fuels. In addition, used as a photocatalytic degradation of organic pollutants. The protocol of model reactions are eco-friendly, efficient, simple and low-cost approach to obtain good to better yield of vitamin B6 analogues 3-deoxypyridoxine (∼92%), C—C coupling products (91%), photo-degradation ($k = 0.1475\ h^{-1}$, c/c_0 and $k = 0.7705\ h^{-1}$, $-\ln c/c_0$) and biodiesel (∼97%). The active 3-deoxypyridoxine intermediate assists to produce synthetically useful scale of other valuable coenzyme synthons, C3 substituted deoxy vitamin B$_6$ of 1-deazaPN, PM, PL, PLNO, PMP and PLP. Moreover, these classes of coenzyme review through density functional theory approach to define quantum chemical process and wave function to support experimental results to emphasize the fundamental properties of activities. Inorganic supported non-toxic heterogeneous nanoparticles draw attention of researchers with broad areas of enzymatic chemistry, industrial chemistry and environmental science.

Acknowledgements

Appendix A. Supplementary data

Supplementary data associated with this article can be found, in the online version, at http://dx.doi.org/10.1016/j.apcatb.2017.03.075.

References

[1] J. Chow, R.J. Kopp, P.R. Portney, Energy resources and global development, Science 302 (2003) 1528–1531.
[2] F. Klose, P. Scholz, G. Kreisel, B. Ondruschka, R. Kneise, U. Knopf, Catalysts from waste materials, Appl. Catal. B: Environ. 28 (2000) 209–221.
[3] H. Zhu, W. Luo, P.N. Ciesielski, Z. Fang, J.Y. Zhu, G. Henriksson, M.E. Himmel, L. Hu, Wood-derived materials for green electronics, biological devices, and energy applications, Chem. Rev. 116 (2016) 9305–9374.
[4] J. Ran, J. Zhang, J. Yu, M. Jaroniec, S.Z. Qiao, Earth-abundant cocatalysts for semiconductor-based photocatalytic water splitting, Chem. Soc. Rev. 43 (2014) 7787–7812.
[5] I. Spiridon, R.N. Darie-Nita, G.E. Hitruc, J. Ludwiczak, I.A. Cianga Spiridon, M. Niculaua, New opportunities to valorize biomass wastes into green materials, J. Clean. Prod. 133 (2016) 235–242.
[6] M.S. Taskhiri, M. Garbs, J. Geldermann, Sustainable logistics network for wood flow considering cascade utilisation, J. Clean. Prod. 110 (2016) 25–39.
[7] R.M. Navarro, M.C. Alvarez-Galvan, J.A. Villoria de la Mano, S.M. Al-Zahrani, J.L.G. Fierro, A framework for visible-light water splitting, Energy Environ. Sci. 3 (2010) 1865–1882.
[8] G.M. Sandala, D.M. Smith, L. Radom, In search of radical intermediates in the reactions catalyzed by lysine 2,3-aminomutase and lysine 5,6-Aminomutase, J. Am. Chem. Soc. 128 (2006) 16004–16005.
[9] A.N. Maity, Y.H. Chen, S.C. Ke, Large- scale domain motions and pyridoxal-5'-phosphate assisted radical catalysis in coenzyme B-12-dependent aminomutases, Int. J. Mol. Sci. 15 (2014) 3064–3087.
[10] A.N. Maity, H.–H. Lin, H.–S. Chiang, H.–H. Lo, S.–C. Ke, Reaction of pyridoxal-5'-phosphate-N-oxide with lysine 5,6-aminomutase: enzyme flexibility toward cofactor analog, ACS Catal. 5 (2015) 3093–3099.
[11] P.A. Frey, G.H. Reed, Pyridoxal-5'-phosphate as the catalyst for radical isomerization in reactions of PLP-dependent aminomutases, Biochim. Biophys. Acta (BBA) Proteins Proteomics 1814 (2011) 1548–1557.
[12] S.J. Abbas, P.V.R.K. Ramacharyulu, S.–C. Ke, MnO2/TiO2 catalyzed synthesis of coenzyme pyridoxamine-5[prime or minute]-phosphate analogues: 3-deoxypyridoxamine-5[prime or minute]-phosphate, RSC Adv. 6 (2016) 10242–10248.
[13] A. Molla, M. Sahu, S. Hussain, Synthesis of tunable band gap semiconductor nickel sulphide nanoparticles: rapid and round the clock degradation of organic dyes, Sci. Rep. 6 (2016) 26034.
[14] M. Rafatullah, O. Sulaiman, R. Hashim, A. Ahmad, Adsorption of methylene blue on low-cost adsorbents: a review, J. Hazard. Mater. 177 (2010) 70–80.
[15] A. Angelis-Dimakis, A. Alexandratou, A. Balzarini, Value chain upgrading in a textile dyeing industry, J. Clean. Prod. 138 (2) (2016) 237–247.
[16] C.A. Martínez-Huitle, E. Brillas, Decontamination of wastewaters containing synthetic organic dyes by electrochemical methods: a general review, Appl. Catal. B: Environ. 87 (2009) 105–145.
[17] C.-C. Wang, J.-R. Li, X.-L. Lv, Y.-Q. Zhang, G. Guo, Photocatalytic organic pollutants degradation in metal-organic frameworks, Energy Environ. Sci. 7 (2014) 2831–2867.
[18] M.L. Marin, L. Santos-Juanes, A. Arques, A.M. Amat, M.A. Miranda, Organic photocatalysts for the oxidation of pollutants and model compounds, Chem. Rev. 112 (2012) 1710–1750.
[19] R. Luque, J.C. Lovett, B. Datta, J. Clancy, J.M. Campelo, A.A. Romero, Biodiesel as feasible petrol fuel replacement: a multidisciplinary overview, Energy Environ. Sci. 3 (2010) 1706–1721.
[20] G.L. Maddikeri, A.B. Pandit, P.R. Gogate, Intensification approaches for biodiesel synthesis from waste cooking oil: a review, Ind. Eng. Chem. Res. 51 (2012) 14610–14628.
[21] A. Karmakar, S. Karmakar, S. Mukherjee, Properties of various plants and animals feedstocks for biodiesel production, Bioresour. Technol. 101 (2010) 7201–7210.
[22] R. Mallampati, S. Valiyaveettil, Eggshell membrane-Supported recyclable catalytic noble metal nanoparticles for organic reactions, ACS Sustain. Chem. Eng. 2 (2014) 855–859.
[23] S.A. Gardezi, B. Joseph, Performance characteristics of eggshell Co/SiO2 Fischer–Tropsch catalysts: a modeling study, Ind. Eng. Chem. Res. 54 (2015) 8080–8092.
[24] M. Nasrollahzadeh, S.M. Sajadi, A. Hatamifard, Waste chicken eggshell as a natural valuable resource and environmentally benign support for biosynthesis of catalytically active Cu/eggshell, Fe3O4/eggshell and Cu/Fe3O4/eggshell nanocomposites, Appl. Catal. B: Environ. 191 (2016) 209–227.
[25] D. Cree, A. Rutter, Sustainable bio-Inspired limestone eggshell powder for potential industrialized applications, ACS Sustain. Chem. Eng. 3 (2015) 941–949.
[26] J. Shen, H. Wang, Y. Zhou, N. Ye, G. Li, L. Wang, Anatase/rutile TiO2 nanocomposite microspheres with hierarchically porous structures for high-performance lithium-ion batteries, RSC Adv. 2 (2012) 9173–9178.
[27] B. Erdem, R.A. Hunsicker, G.W. Simmons, E.D. Sudol, V.L. Dimonie, M.S. El-Aasser, XPS and FTIR surface characterization of TiO2 particles used in polymer encapsulation, Langmuir 17 (2001) 2664–2669.
[28] S. Nath, S. Kumar Ghosh, S. Praharaj, S. Panigrahi, S. Basu, T. Pal, Silver organosol: synthesis, characterisation and localised surface plasmon resonance study, New J. Chem. 29 (2005) 1527–1534.
[29] Y. Castro, N. Arconada, A. Durán, Synthesis and photocatalytic characterisation of mesoporous TiO$_2$ films doped with Ca, W and N, Boletín de la Sociedad Española de Cerámica y Vidrio 54 (2015) 11–20.
[30] R.G. Jones, E.C. Kornfeld, Lithium aluminum hydride reduction of pyridine carboxylic esters: synthesis of vitamin B6, J. Am. Chem. Soc. 73 (1951) 107–109.
[31] R.K. Blackwood, G.B. Hess, C.E. Larrabee, F.J. Pilgrim, The synthesis of 6-Chloropyridoxine. the hydride reduction of pyridinedicarboxylic acids, J. Am. Chem. Soc. 80 (1958) 6244–6249.
[32] N.A. Stambolieva, Y.N. Breusov, M.Y. Karpeisky, A.M. Kritzyn, V.L. Florentiev, Analogues of vitamin B6: synthesis and properties of 3-deoxypyridoxal phosphate and 3-O-methylpyridoxal phosphate, Tetrahedron 26 (1970) 3083–3090.
[33] R. Madhuvilakku, S. Piraman, Biodiesel synthesis by TiO2–ZnO mixed oxide nanocatalyst catalyzed palm oil transesterification process, Bioresour. Technol. 150 (2013) 55–59.
[34] Z. Wen, X. Yu, S.-T. Tu, J. Yan, E. Dahlquist, Biodiesel production from waste cooking oil catalyzed by TiO2–MgO mixed oxides, Bioresour. Technol. 101 (2010) 9570–9576.
[35] B. Jiang, M. Xu, Highly enantioselective construction of fused pyrrolidine systems that contain a quaternary stereocenter: concise formal synthesis of (+)-conessine, Angew. Chem. 116 (2004) 2597–2600.
[36] A. Hoepping, K.M. Johnson, C. George, J. Flippen-Anderson, A.P. Kozikowski, Novel conformationally constrained tropane analogues by 6-endo-trig radical cyclization and stille coupling-switch of activity toward the serotonin and/or norepinephrine transporter, J. Med. Chem. 43 (2000) 2064–2071.
[37] J.J. Fleming, J. Du Bois, A synthesis of (+)-saxitoxin, J. Am. Chem. Soc. 128 (2006) 3926–3927.
[38] W. Lin, T. Cao, W. Fan, Y. Han, J. Kuang, H. Luo, B. Miao, X. Tang, Q. Yu, W. Yuan, J. Zhang, C. Zhu, S. Ma, Enantioselective double manipulation of

tetrahydroisoquinolines with terminal alkynes and aldehydes under copper(I) catalysis, Angew. Chem. Int. Ed. 53 (2014) 277–281.

[39] M. Naoi, W. Maruyama, H. Yi, K. Inaba, Y. Akao, M. Shamoto-Nagai, Mitochondria in neurodegenerative disorders: regulation of the redox state and death signaling leading to neuronal death and survival, J. Neural Transm. 116 (2009) 1371–1381.

[40] W. Maruyama, Y. Akao, M.C. Carrillo, K.I. Kitani, M.B.H. Youdium, M. Naoi, Neuroprotection by propargylamines in Parkinson's disease: suppression of apoptosis and induction of prosurvival genes, Neurotoxicol. Teratol. 24 (2002) 675–682.

[41] J.P. Brand, J. Waser, Electrophilic alkynylation: the dark side of acetylene chemistry, Chem. Soc. Rev. 41 (2012) 4165–4179.

[42] D. Habrant, V. Rauhala, A.M.P. Koskinen, Conversion of carbonyl compounds to alkynes: general overview and recent developments, Chem. Soc. Rev. 39 (2010) 2007–2017.

[43] H. Nakamura, T. Kamakura, M. Ishikura, J.-F. Biellmann, Synthesis of allenes via palladium-catalyzed hydrogen-transfer reactions: propargylic amines as an allenyl anion equivalent, J. Am. Chem. Soc. 126 (2004) 5958–5959.

[44] S.P. Teong, D. Yu, Y.N. Sum, Y. Zhang, Copper catalysed alkynylation of tertiary amines with CaC2 via sp3 CH activation, Green Chem. 18 (2016) 3499–3502.